

NEDO-25116  
79NED105  
CLASS I  
AUGUST 1979

**MK II MHM COMPARED WITH  
PRELIMINARY RESULTS FROM  
SM TEST PROGRAM**

*POOR ORIGINAL*

A. P. REESE

1185 143

7910180 226

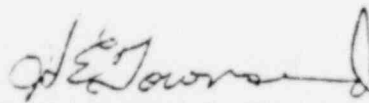
GENERAL  ELECTRIC

NEDO-25116  
79NED105  
Class I  
August 1979

A COMPARISON OF THE MARK II MULTIVENT  
HYDRODYNAMIC MODEL WITH PRELIMINARY  
RESULTS FROM THE SCALED MULTIVENT TEST PROGRAM

A. P. Reese

Reviewed:



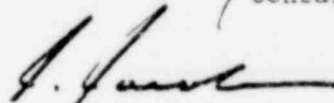
H. E. Townsend, Manager  
Containment Methods

Approved:



A. E. Rogers, Manager  
Containment Technology

Approved:



J. Jacobson, Manager  
Reactor and Containment Design

1185 144

## DISCLAIMER OF RESPONSIBILITY

Neither the General Electric Company nor any of the contributors to this document makes any warranty or representation (express or implied) with respect to the accuracy, completeness, or usefulness of the information contained in this document or that the use of such information may not infringe privately owned rights; nor do they assume any responsibility for liability or damage of any kind which may result from the use of any of the information contained in this document.

1185 145

## TABLE OF CONTENTS

	<u>Page</u>
ABSTRACT	v
1. INTRODUCTION	1-1
1.1 Objective	1-1
1.2 Strategy	1-1
1.3 Model Modifications	1-2
2. CONCLUSIONS	2-1
3. ENGINEERING MODELS	3-1
3.1 Hydrodynamic Model - Method of Images	3-1
3.1.1 Theory and Assumptions	3-1
3.1.2 Determination of Source Strength $\dot{q}_r$	3-4
3.2 Monte-Carlo Methods	3-4
3.2.1 Chug Library Design	3-5
3.2.2 Vent-Chug Assignment	3-5
3.2.3 Chug Asynchronization	3-5
3.2.4 Statistical Analysis	3-6
4. RESULTS AND DISCUSSION	4-1
4.1 Comparison of Predicted to Measured Multivalent Multipliers	4-2
4.2 Sensitivity to Asynchronization Bandwidth	4-3
APPENDICES	
A. CALCULATION OF PRESSURE FACTORS	A-1
B. SENSITIVITY OF IMAGE METHOD TO NODE NUMBER AND IMAGINARY SOURCE POSITION	B-1

## LIST OF TABLES

<u>Table</u>	<u>Title</u>	<u>Page</u>
1-1	Thermodynamic Conditions Used for test Comparisons	1-3
4-1	Comparison of POP and PUP Statistics of Original Tapes and Final Chug Libraries	4-5
4-2	Phasing Results from 3 Vent Tests	4-6
4-3	Inputs for chugging Probabilities for the Seven Vent Runs	4-6
4-4	Mean POP and PUP Data from Multivent Test	4-7
4-5	Mean POP and PUP Predicted by MHM	4-7
4-6	Mean POPs and PUPs when all Vents Chug	4-8

## LIST OF ILLUSTRATIONS

<u>Figure</u>	<u>Title</u>	<u>Page</u>
1-1	Image Pattern to Simulate Boundary Effects in a Vertical Radial Cross Section of Mark II Pool	1-4
1-2	Image Geometry of Mark II Pool	1-5
1-3	Geometry of 7 Scaled Multivent Test Vessels Used for Comparisons	1-6
3-1	Location of Nodes and Imaginary Sources	3-7
3-2	Multivent Source Array	3-8
4-1	Comparisons of Real Asynchronization Distribution with that used in the MHM	4-9
4-2	Test Series 2420, Asynchronization 19.5 msec	4-10
4-3	Test Series 2620, Asynchronization 33 msec	
4-4	Test Series 3420, Asynchronization 12.5 msec	
4-5	Test Series 3620, Asynchronization 40 msec	
4-6	Predicted versus Measured Multivent Multipliers, Assigned Chug Participation	
4-7	Measured versus Predicted Multivent Multipliers, all Vent Participation	
4-8	Test Series 2420, Sensitivity to Asynchronization	4-11
4-9	Test Series 2620, Sensitivity to Asynchronization	4-12
4-10	Test Series 3420, Sensitivity to Asynchronization	4-13
4-11	Test Series 3620, Sensitivity to Asynchronization	4-14

## ABSTRACT

*In order to determine the wall pressures on a Mark II containment system during the chugging phase of a postulated LOCA, a model was developed which employs single vent chugging data and a Monte-Carlo technique to simulate multivent effects. This method utilizes a potential flow solution to predict containment wall pressures from vent source strengths. This report quantifies the performance of this model by comparing model predictions to results of sub-scale multivent chugging tests.*

## 1. INTRODUCTION

### 1.1 OBJECTIVE

One method for calculating chugging loads in Mark II containments consists of using measured pressure histories from the 4T full scale single cell tests as inputs to a Multivent Hydrodynamic Model (MHM).<sup>\*</sup> The randomness of the chugging phenomenon is taken into account by use of Monte-Carlo techniques to randomly select chugs and synchronization times. 4T pressure histories are used to generate chugging source strengths using potential flow theory. These source histories are then randomly assigned to the ends of each of the downcomers and a potential flow solution with superposition is then used to calculate the applied containment wall pressure histories.

The objective of this report is to develop a preliminary assessment of the validity of the assumptions and techniques employed and to show that the potential flow solution is a reasonable approximation to the actual pressure propagation within the suppression pool.

This effort is one element of the Mark II Containment Long Range Program (Task A.11 Phase 3A). This task is designed to give early indications of the model validity by making comparisons with a limited number of test data points.

### 1.2 STRATEGY

The verification of the MHM consists of comparisons between the multivent multiplier<sup>†</sup> curves predicted by the model, and data from the Scaled Single and Multivent Test Program (Mark II Long Range Program Task A.11 Phase 1.\*\* The comparisons were made for 3 and 7 vents at 1/10 scale for a range of conditions which include four different combinations of vent steam mass flux and wetwell overpressure. Table 1-1 shows the test series used in the comparisons and their thermodynamic conditions.

<sup>\*</sup>S. A. Wilson, et al., "The Multivent Hydrodynamic Model for Calculating Pool Boundary Loads due to Chugging - Mark II Containment," NEDC-21699-P, February 1978.

<sup>\*\*</sup>W. J. Clabaugh, "Scaled Multivent Test Program Plan (Phase 1 Tests)," NEDO-23697A, January 1979.

<sup>†</sup>The multivent multiplier is defined as the ratio of multivent to single vent chugging mean peak over or under pressures.

### 1.3 MODEL MODIFICATIONS

To generate multivent multipliers for the comparisons, the MHM was modified slightly to account for the test vessel geometry. The solution of the potential flow equation is performed by a classical method of images, subject to boundary conditions dictated by the Mark II geometry. The imaging approach used for prototype MK II containments is illustrated in Figures 1-1 and 1-2. As shown in these figures, the Mark II pool is treated as a rectangular trough, with the "unrolled" containment shell and reactor pedestal forming the two walls. This geometry is very different from that of the vessels used in the Subscale Multivent Test Program, which utilize close packed hexagonal unit cells in cylindrical tanks, as shown in Figure 1-3. A different imaging method, therefore, is implemented into the MHM. This method is fully described in Subsection 2.1.

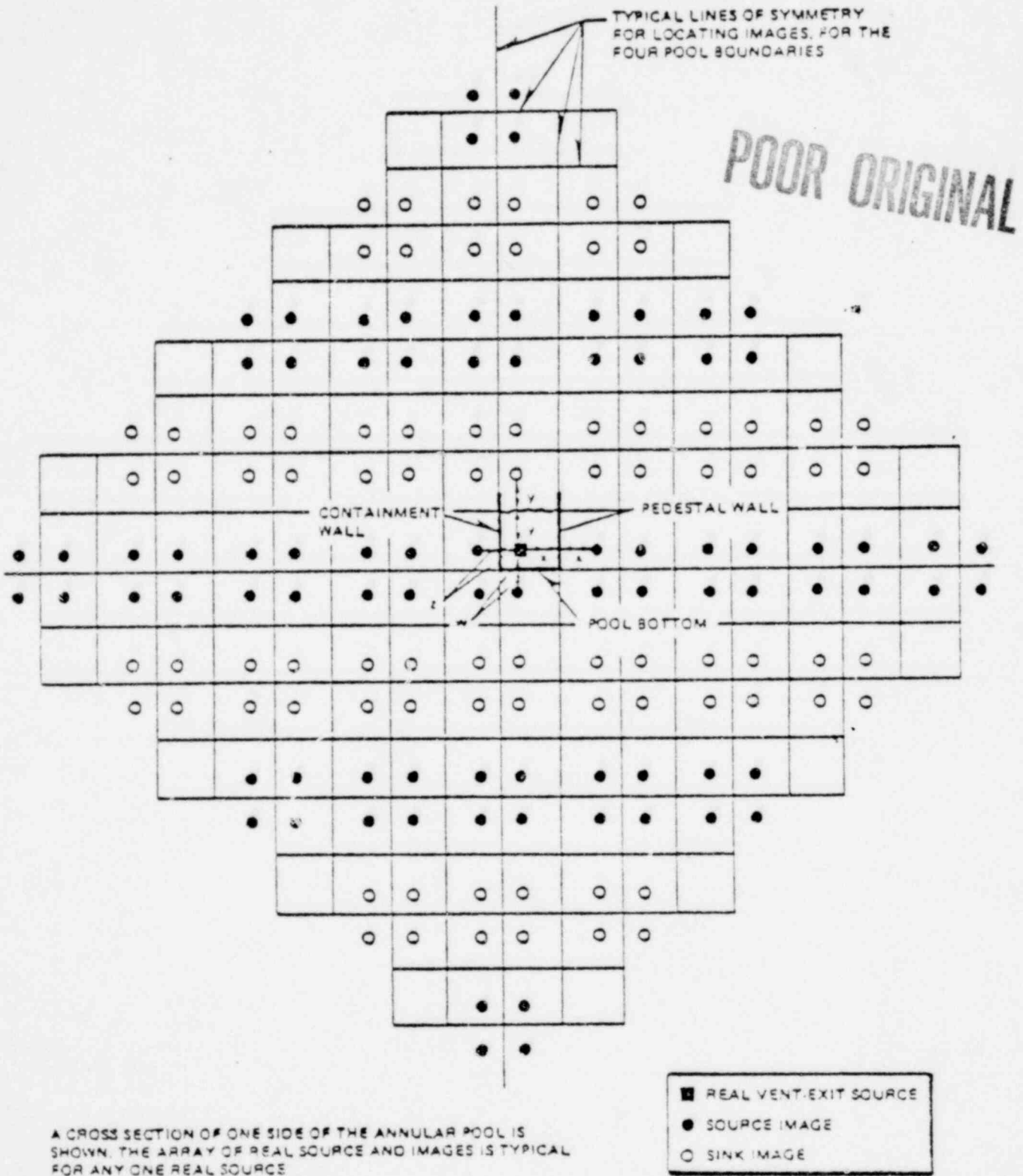
A change is also made in the Monte-Carlo portion of the MHM, in order to more correctly simulate the test conditions. The MHM is designed to predict loads resulting from "pool chugs," that is, events in which all vents chug at very nearly the same time. In the chugging tests, however, it was observed that during some pool chugs not all of the vents participated. Thus, the MHM was given the ability to model these "partial pool chugs," by inputting different vent chugging probabilities.

Again, this refinement is made to better model the actual phenomenon. Results are compared to "full pool chug" runs to show that they are bounding. This methodology is described fully in Subsection 3.2.2.

It should be mentioned that the frequency transfer of the 4T source strengths which was necessary when predicting Mark II loads from 4T single cell chugging source strengths is not necessary for these comparisons. The frequency transfer is not required because, unlike the 4T and prototype, both the single vent data, and the multivent data being predicted from it, share the same geometric and thermodynamic conditions. In particular, scale, vent mass flux, air content, wetwell overpressure, pool temperature, and acoustic path lengths are common to both the single vent data used as source strengths and the multivent data which is being predicted.

Table 1-1  
THERMODYNAMIC CONDITIONS USED FOR TEST COMPARISONS

<u>Test Series Number</u>	<u>Mass Flux (lbm/ft<sup>2</sup>-sec)</u>	<u>Wetwell Overpressure (psia)</u>	<u>Pool Temperature (°F)</u>
2420	1.0	14.7	90
2620	4.0	14.7	90
3420	1.0	45.0	90
3620	4.0	45.0	90



A CROSS SECTION OF ONE SIDE OF THE ANNULAR POOL IS SHOWN. THE ARRAY OF REAL SOURCE AND IMAGES IS TYPICAL FOR ANY ONE REAL SOURCE

- REAL VENT-EXIT SOURCE
- SOURCE IMAGE
- SINK IMAGE

Figure 1-1. Image Pattern to Simulate Boundary Effects in a Vertical Radial Cross Section of Mark II Pool



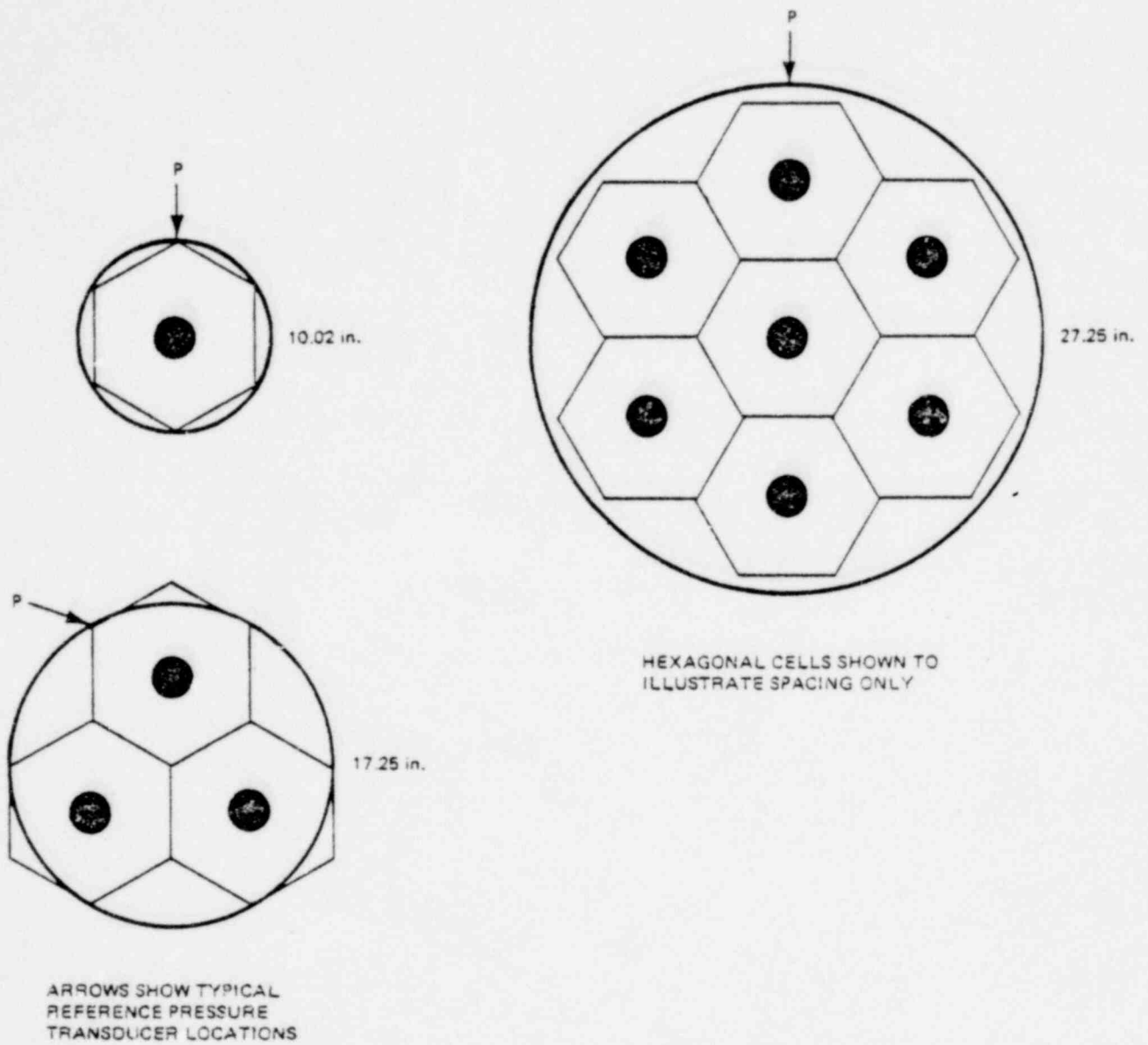


Figure 1-3. Geometry of 7 Scaled Multivalent Test Vessels Used for Comparisons

2. CONCLUSIONS AND SUMMARY

The results of the data comparisons and sensitivity studies indicate that the following statements can be made about the performance of the MHM:

- a. The MHM is successful in predicting the general trends of the multivent test data. The continuing decrease of the multivent multiplier with increasing number of vents is seen in all cases.
- b. When using the MHM in the "all vents chugging" mode, as used for the prototype, it generally predicts conservative multivent multipliers. However, when using measured vent chugging probabilities<sup>+</sup> the MHM tends to underpredict the multivent multiplier by 10-20 percent.
- c. The MHM produces peak pool boundary pressures which are nearly insensitive to the asynchronization\* above some critical value, usually about 10 msec. The multivent multipliers predicted by the MHM go to unity as the asynchronization goes to zero.

---

<sup>+</sup> The measured probability of one, two, or three vents chugging in a given pool chug (see Subsection 3.2.2).

\* Asynchronization is the period of time between the 1st and last individual vents to chug within a given pool chug (see Subsection 3.2.3).

1185 157

### 3. ENGINEERING MODELS

#### 3.1 HYDRODYNAMIC MODEL - METHOD OF IMAGES

In order to transfer vent source strengths into wall pressures, a hydrodynamic model using a potential flow formulation, solved by a method of images is employed. Source strengths and characteristics are obtained from single vent test data.

##### 3.1.1 Theory and Assumptions

The following assumptions are made in this hydrodynamic model:

- a. The fluid in the vessel is incompressible and inviscid;
- b. The fluid velocities are small;
- c. The vessel walls are perfectly rigid.

Assumption a leads to the application of the potential flow formulation, and the pressure distribution in the vessel can be determined from the transient Bernoulli equation:

$$-\rho \frac{\partial \phi}{\partial t} + \rho \frac{(\Delta \phi)^2}{2} + P - P_{\infty} = 0 \quad (1)$$

where  $P_{\infty}$  is the static pressure at the point of interest in the vessel,  $P$  is the dynamic pressure at that point,  $\rho$  is the fluid density, and  $\phi$  is the velocity potential.

Because inertia effects are small (assumption b) the second term of equation 1 can be neglected

$$P - P_{\infty} = \rho \frac{\partial \phi}{\partial t} \quad (2)$$

The growth and collapse of steam bubbles at the end of the vents are represented by time varying point sources (at the location of the vent exit) which can be described by the velocity potential

$$\phi = \frac{q}{4\pi r} \quad (3)$$

where:

$q$  = volume flow rate, a function of time.

$r$  = distance from the source to the point of interest.

Substituting equation 3 into equation 2

$$P - P_{\infty} = \frac{\dot{q}}{4\pi r} \quad (4)$$

The effect of the vessel walls is simulated by creating an array of imaginary sources around the outside of the vessel. These imaginary sources, located about one vessel diameter from the vessel walls, are arranged uniformly around the vessel sides and below the vessel bottom. The effect of the free surface is accounted for by the addition of a sink of equal magnitude corresponding to each source, both real (inside the vessel) and imaginary (outside the vessel), at the corresponding distance above the plane of the free surface. A set of linear equations is developed which describe the fluid velocity at certain points (nodes) on the vessel walls as a function of the imaginary source strengths.

These equations are solved for the imaginary source strengths which satisfy the rigid boundary condition of zero normal velocity at each node. Once all source strengths are determined, the pressure due to each source at a point of interest on the test vessel wall is found from equation 4. The resulting pressure at this point is the sum of the pressure contributions due to all sources. The general arrangement of real sources, imaginary sources, nodes and source reflections for a scaled multivent test vessel is shown in Figure 3-1.

A detailed derivation of the image method is given in Appendix A. The analysis shows that the pressure contribution from any one vent source at a given point in the pool is directly proportional to the source strength. Also, the pressure due to several sources is the algebraic sum of the pressure contributions of each individual source. Thus the pressure is given by:

$$P - P_{\infty} = \sum_{i=1}^{nv} f_i q_{Ri} \quad (5)$$

where:

$f_i$  = pressure factor of the  $i$ th vent

$q_{Ri}$  = source strength for the  $i$ th vent

$nv$  = number of vents.

Equation (5) can be written in matrix notation as

$$P - P_{\infty} = F Q_r \quad (5)$$

where:

$$F = [f_1, f_2, \dots, f_{nv}]$$

$$Q_r = [q_{r1}, q_{r2}, \dots, q_{rnv}]^T$$

The MHM first uses the imaging method to calculate the pressure factor vector,  $F$ . The Monte-Carlo portion of the calculation is then entered. Here a source strength vector,  $Q_r$ , is calculated at each time step and multiplied by the pressure factor vector to obtain the desired wall pressure.

### 3.1.2 Determination of the Source Strength, $\dot{q}_r$

The source strengths  $\dot{q}_{r1}$ , used in equation 5 are determined from wall pressure measurements taken during subscale single vent chugging tests. For the case of the single vent vessel the pressure factor vector,  $F$ , is a single number denoted  $f_1^{(sv)}$ , and is found by running the MMH in the single cell mode, which is identical to the multicell mode, but with only a single source. The source strength is found using a single vent version of equation 5:

$$\dot{q}_r^{(sv)} = \frac{(P - P_\infty)_{\text{measured}}}{f_1^{(sv)}} \quad (7)$$

Input to the program consists of time histories of single vent chugging pressure and the single vent pressure factor  $f_1^{(sv)}$ . These pressure histories, converted to source strengths by  $f_1^{(sv)}$ , are placed in the multivalent source array,  $Q_r$ , using Monte-Carlo techniques (Section 3.2). The resulting multivalent wall pressure history is then computed using equation 6.

### 3.2 MONTE-CARLO METHODS

The Monte-Carlo methods used in this evaluation model are identical to those used in the MMH with the additional ability of generating partial pool chugs according to given probabilities. The Monte-Carlo portion of the analysis consists of 200 pool chug trials. A trial consists of first generating a multivalent source array from a library of single vent pressure histories, then using equation 5 of Subsection 3.1.1 to find the resulting multivalent pressure history. The peak overpressure (POP), and peak underpressure (PUP), of this pressure history are found, and the next trial then begins. Upon the completion of the 200 trials a statistical analysis is performed on the resulting POPs and PUPs.

A more complete description of the Monte-Carlo methods used may be found in

1185 161

### 3.2.1 Chug Library Design

A chug library is developed from wall pressure measurements from the single vent chugging facility for each of the thermodynamic conditions listed in Table 1-2. As discussed in Section 1.3 no frequency transfer of the pressure histories is necessary.

Each library has 54 chugs consisting of 768 data points each, 0.1 msec apart. The maximum positive pressure of each chug is always set at the midpoint (382th time step) of the chug.

The 54 chugs of each library were picked from a complete pressure history of each single vent test. All tests were run for ~80 seconds, and during this period, a different number of chugs developed depending on the thermodynamic conditions. The 54 chugs used in each library were chosen from all the available chugs so that the peak overpressure and underpressure statistics were representative of the complete sample.

### 3.2.2 Vent-Chug Assignment

At the beginning of each trial the number of vents which will participate is determined. This number is chosen at random from a given probability distribution. These distributions were determined from data taken in the 3 vent 1/10th scale facility, at the same thermodynamic conditions as the single vent case. This number of chugs is then randomly drawn from the chug library. Reselection of chugs is permitted. The chugs are then randomly assigned to vents and the vents not assigned a chug are given a "zero chug."

### 3.2.3 Chug Asynchronization

Once the vents have been assigned chugs, the chugs are then asynchronized in time. An asynchronization time is chosen for each chug at random from a flat distribution. The chugs are then placed into the multivent source array in accordance with their respective asynchronization times. Figure 3-2 illustrates this process for three vents. The dotted lines indicate the positions of chugs

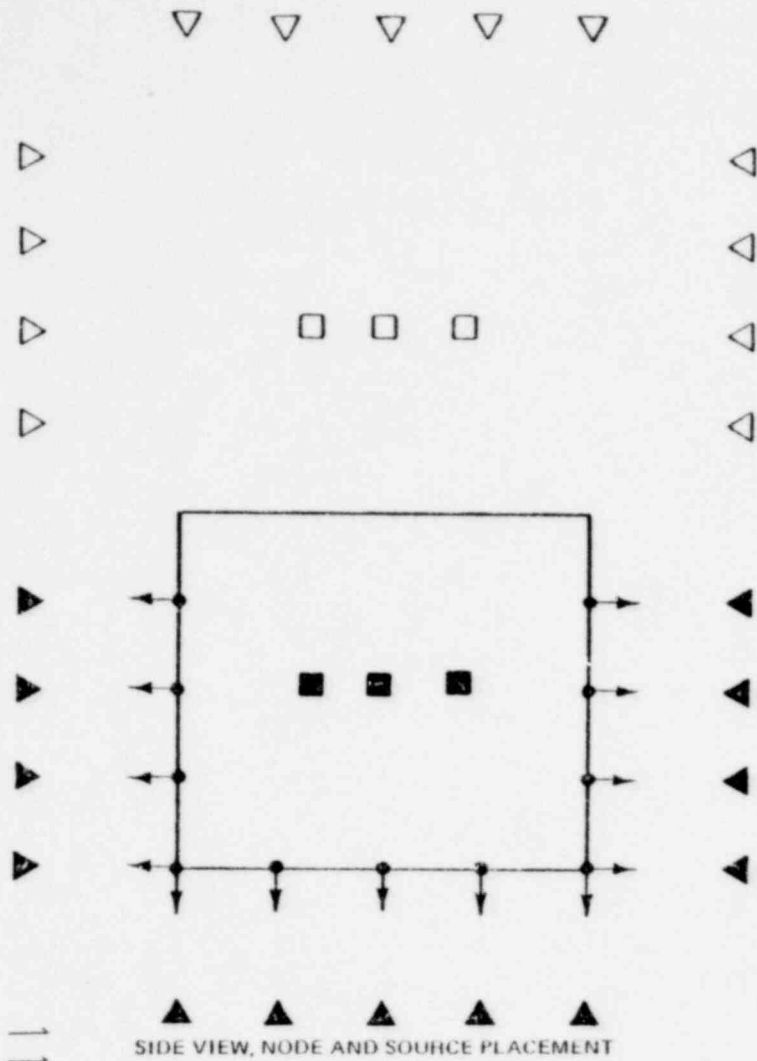
before being asynchronized, while the solid lines show the final positions of the chugs in the source array.

The bandwidth from which the asynchronization times are drawn is determined from the observed asynchronization of chugs in the 3 vent 1/10th scale facility at the same thermodynamic conditions as the single vent cases. Chug asynchronization is the last step in the generation of the course strength vector,  $Q_r$ .

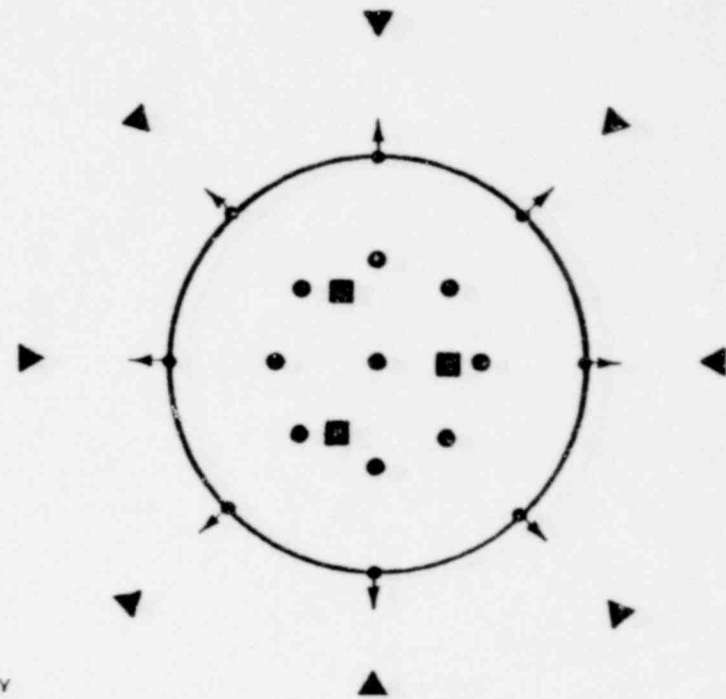
#### 3.2.4 Statistical Analysis

Once the source vector is generated, equation 5 of Subsection 3.1.1 is used to evaluate the resulting pressure history. This history is then searched in order to determine the peak overpressure and underpressure. The POPs and PUPs resulting from all the trials are then analyzed to determine their mean values, maximum values, and standard deviations. Histograms of the POP and PUP distributions are also developed.

1185 163



SIDE VIEW, NODE AND SOURCE PLACEMENT



TOP VIEW, NODE AND SOURCE PLACEMENT

- KEY
- NODE
  - REAL SOURCE
  - REAL SOURCE REFLECTION
  - ▲ IMAGINARY SOURCE
  - △ IMAGINARY SOURCE REFLECTION
  - ↑ NORMAL VECTOR

Figure 3-1. Location of Nodes and Imaginary Sources

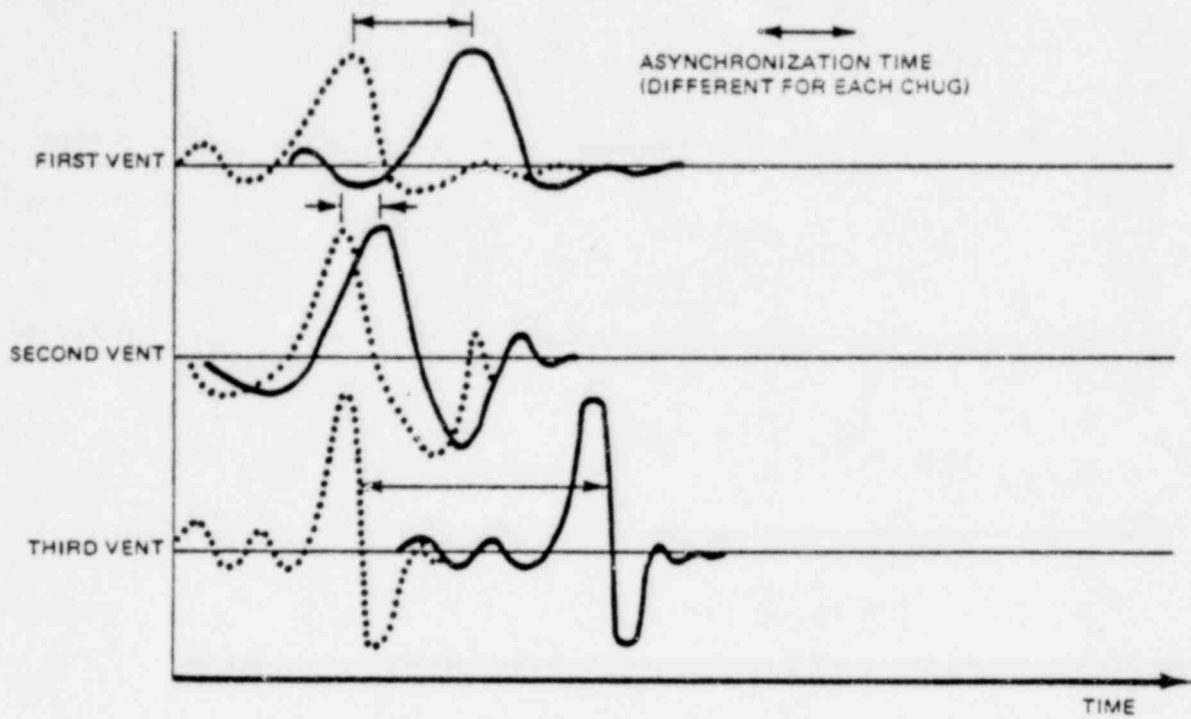


Figure 3-2. Multivent Source Array

#### 4. RESULTS AND DISCUSSION

The modified MHM was used to predict multivalent multipliers as a function of the number of vents for the four tests at different thermodynamic conditions shown in Table 1-2. Four different chug libraries (see Subsection 3.2.1) were developed from digitized tapes of the single vent tests. Two of the four tests yielded significantly more chugs than were needed for the libraries, so the data was reviewed and 54 representative chugs chosen so as to match the statistics of the original data sample and the chug library. In particular, the maximum chug in each data sample was included in the chug library for that run. The other two tests used essentially the entire data sample in the chug libraries.

In order to determine how well the chug libraries characterized the chugs of the original data samples, each library was run in the MHM, set up in the single vent geometry. In this way the MHM was used to search the chugs of the chug libraries for the peak overpressures (POPs) and underpressures (PUPs) and then to run a statistical analysis on them. The results of these runs, together with the statistics from the original tapes are shown in Table 4-1.

As may be seen from Table 4-1, reasonably good agreement was obtained between the original data samples and the chug libraries, particularly for tests 2420, 3420, and 3620, where the difference between the means of the original data and libraries averages less than 4%. Differences in the peaks are similar. The comparisons for test 2620 is not as good, with a difference of more than 15% on the mean. It should be emphasized that these differences are due not to the chug selection used (tests 2420 and 3420 used virtually the entire data sample in the library) but to differences in data reduction technique (for example fixed vs floating trend removal) and the computer systems used for analysis.

The vents of the 3-vent test model were instrumented so that chugging probability and vent phasing data could be obtained. The data obtained for each of the four test conditions is summarized in Table 4-2. In this table the column labeled "P-1 vent" is the probability that only one vent will

participate in a pool chug, "P-2 Vent" is the probability that 2 vents will participate in a pool chug, and so on. Asynchronization in the last column is the mean time between the first and last chug of a pool chug.

The asynchronization bandwidth (see Subsection 3.2.3) used as input to the MHM was chosen as the mean plus one standard deviation found in the 3 vent test. The same bandwidth was used for three and seven vent runs. The rationale for choosing the bandwidth this way is illustrated in Figure 4-1. The asynchronization statistic shown in Table 4-2, with standard deviation approximately equal to the means, indicate distributions highly shifted to the low end but with relatively long tails on the high end. Thus a flat distribution from zero to the mean plus one standard deviation is a good approximation to the real distribution.

The numbers in the first three columns of Table 4-2 were used directly as input to the MHM for the vent chugging probability distribution (see Subsection 3.2.2). Because only three vents of the 7 vent test were instrumented probability data was inferred from the 3 vent data. Table 4-3 shows the inputs used for the chugging probability distribution for the four 7-vent tests. The strategy here was to keep the same relative probability ratios of vents chugging in seven vents as in three vents.

#### 4.1 COMPARISON OF PREDICTED TO MEASURED MULTIVENT MULTIPLIERS

The preliminary mean POPs and mean PUPs found in the three and seven vent tests for the four thermodynamic conditions are shown in Table 4-4. Uncertainty analyses are not yet complete, but the initial estimate of the uncertainty is about  $\pm 0.5$  psi. The results of the three and seven vent MHM runs for the four thermodynamic conditions are shown in Table 4-5.

The multivent multipliers as a function of vent number are found from this data by dividing the 3 and 7 vent results by the single vent data. The multipliers thus obtained are shown by the solid lines in Figures 4-2 through 4-5. The test results and uncertainty bands are also shown on these figures. As seen the MHM was successful in predicting the general trend of the

multivent multiplier. In all cases the multiplier decreases with increasing number of vents. Figure 4-6 shows a comparison of all multipliers predicted by the MHM versus those measured. The MHM seems to have a slight tendency to underestimate the data. This underestimation, however, is never more than 10 percent except in the case of the 2620 series tests. As discussed earlier, there is some reason to doubt the accuracy of the chug library used for this test series.

The MHM was also run with the vent chugging probabilities set so that all vents chug each trial. This is the methodology used in the Mark II MHM. The mean POPs and PUPs obtained in this series of runs are shown in Table 4-6.

The multivent multipliers as a function of vent number for these runs are shown by the broken lines in Figures 4-1 through 4-5. As expected the multivent multiplier found with full vent chugging are always greater than those found when applying measured chugging probabilities. The predicted versus measured multipliers found in these runs are shown in Figure 4-7. Run in this way the MHM is generally found to be conservative.

#### 4.2 SENSITIVITY TO ASYNCHRONIZATION BANDWIDTH

The effect of varying the asynchronization bandwidth was determined by using different bandwidths from 0 to 40 msec, for each chug library, for both 3 and 7 vents. The case of all vents participating in each trial was used for these studies. The multivent multiplier versus asynchronization as shown in Figure 4-8 through 4-11. As seen, the MHM is only slightly sensitive to asynchronization above 15 msec for the 2420 and 2620 runs and 5 msec for the 3420 and 3620 runs. Below these critical values the POPs are very sensitive to asynchronization. This is a consequence of the way in which the chug libraries are designed, with the POPs assigned at the mid-point in each chug.

In the case of zero asynchronization (all vents in phase), Figures 4-8 through 4-11 show that the multivent multipliers based on the peak overpressures goes to unity, as expected. This result is not seen in the underpressures, however, which tend to a value of about 0.8 at zero asynchronization. This

result comes about because of the way the single vent libraries were generated, with the POP centered in the time duration of the chug. Asynchronization is based on the time between peak overpressures for the chugs assigned to each vent. Thus, for an asynchronization of zero, all vents have a peak overpressure at the same instant in time. For the underpressures, however, different chugs in the single vent library will have the peak underpressures at different times relative to the peak overpressures. Thus with the asynchronization equal to zero, different vents participating in a pool chug will have their individual peak underpressures occurring at different points in time, even though the overpressures are synchronized. If the chug libraries were developed with the underpressures centered in each chug, so that the underpressure asynchronization could be set to zero, it is expected that a unity multivent multiplier for underpressures would result.

Table 4-1  
COMPARISON OF POP AND PUP STATISTICS OF ORIGINAL TAPES AND FINAL CHUG LIBRARIES

\*

\*Bars drawn in the margin of the text of this report indicates proprietary information of the General Elcetric Company.

Table 4-2  
PHASING RESULTS FROM 3 VENT TESTS

Probability of Vent Participation

Asynchronization

Table 4-3  
INPUTS FOR CHUGGING PROBABILITIES FOR  
THE SEVEN VENT RUNS

Probability of Vent Participation

\*Bars drawn the margin of the text of this report indicate proprietary information of the General Electric Company.

Table 4-4

MEAN POP AND PUP DATA FROM MULTIVENT TEST

Table 4-5

MEAN POP AND PUP PREDICTED BY MHM

Table 4-6

MEAN POPS AND PUPS WHEN ALL VENTS CHUG

<u>Test</u>	<u>2420</u>		<u>2620</u>		<u>3420</u>		<u>3620</u>	
	<u>POP</u>	<u>PUP</u>	<u>POP</u>	<u>PUP</u>	<u>POP</u>	<u>PUP</u>	<u>POP</u>	<u>PUP</u>
1 Vent	5.72	-4.13	17.78	-6.90	6.53	-6.13	14.88	-9.25
3 Vent	3.50	-2.71	9.11	-4.46	4.78	-4.22	12.26	-6.47
7 Vent	2.01	-1.72	4.87	-2.93	2.72	-2.58	7.90	-4.07

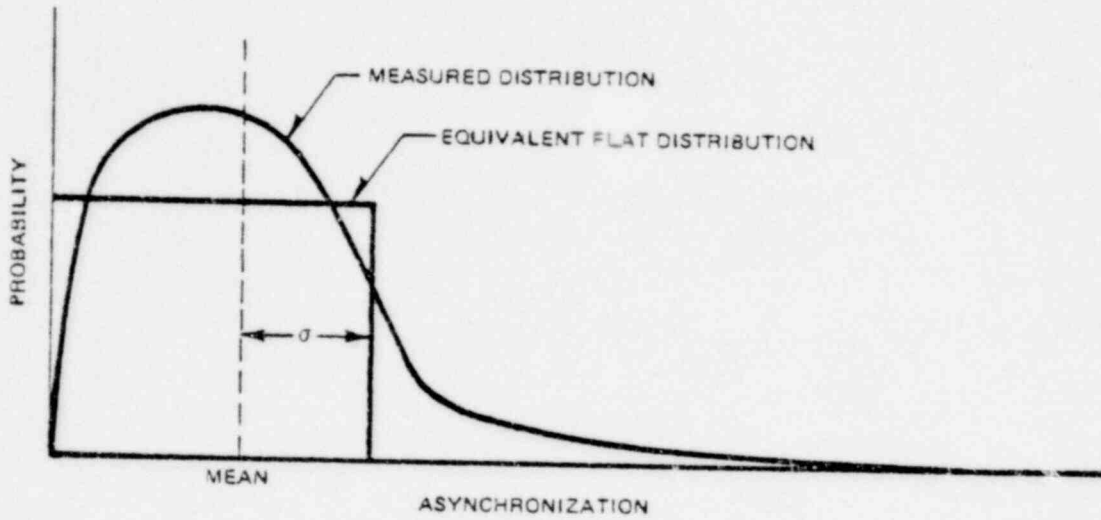


Figure 4-1. Comparison of Real Asynchronization Distribution with that used in the MHM

The following figures are GE COMPANY PROPRIETARY and have been removed from this document in their entirety.

Figure 4-2. Test Series 2420, Asynchronization 19.5 msec

Figure 4-3. Test Series 2620, Asynchronization 33 msec

Figure 4-4. Test Series 3420, Asynchronization 12.5 msec

Figure 4-5. Test Series 3620, Asynchronization 40 msec

Figure 4-6. Predicted versus Measured Multivent Multiplier,  
Assigned Chug Probabilities

Figure 4-7. Measured versus Predicted Multivent Multipliers,  
all Vents Participating

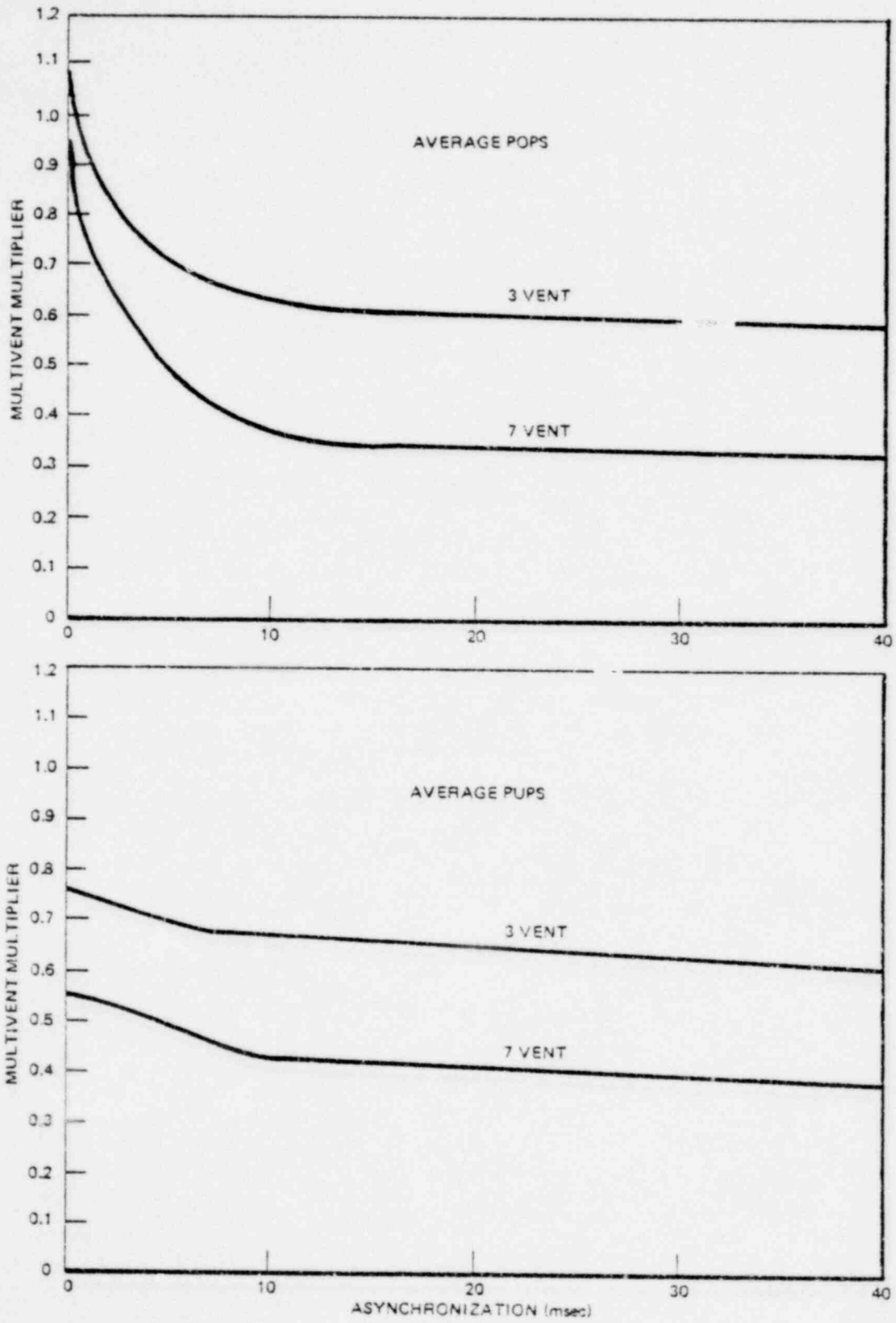


Figure 4-8. Test Series 2420, Sensitivity to Asynchronization

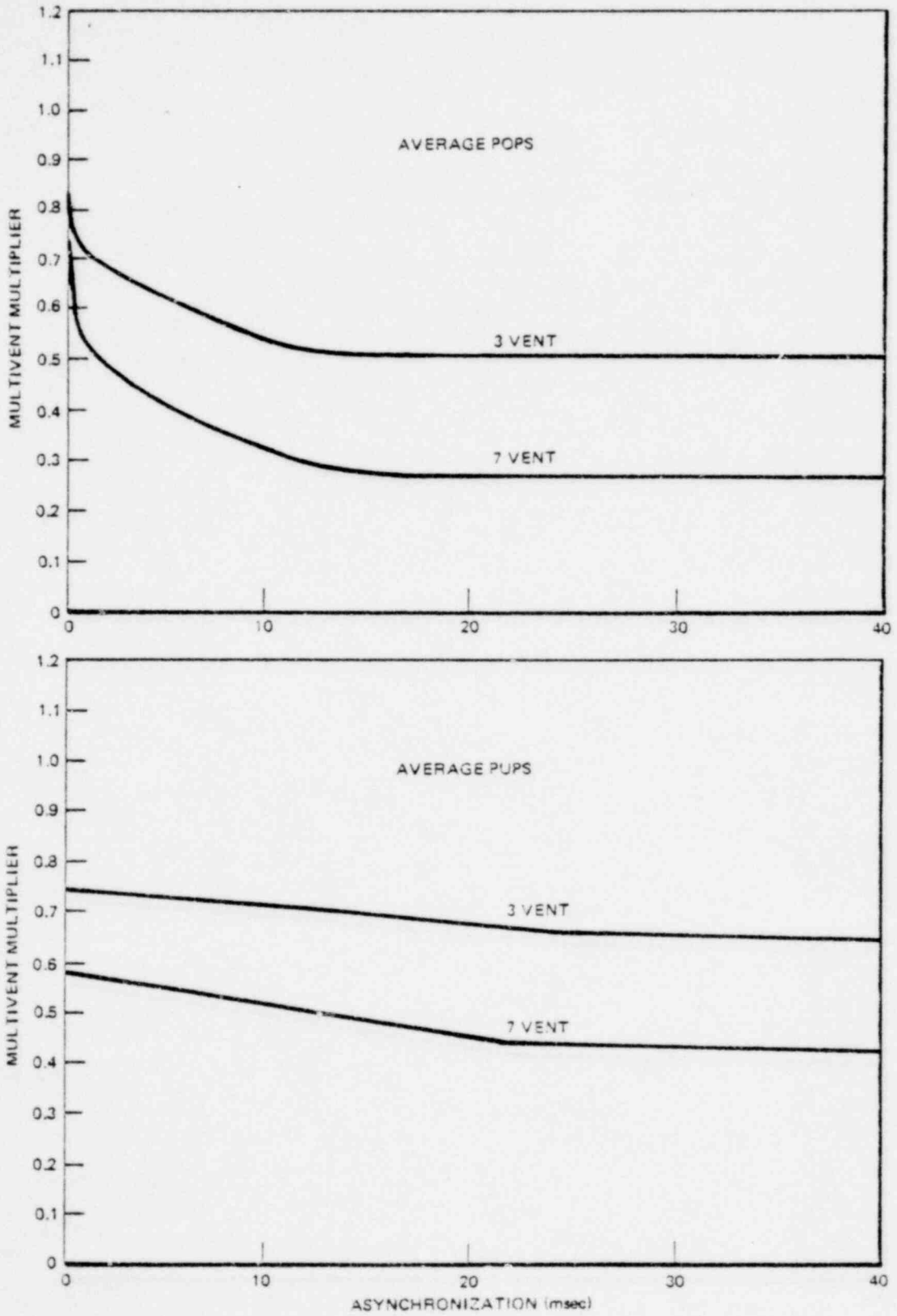


Figure 4-9. Test Series 2620, Sensitivity to Asynchronization

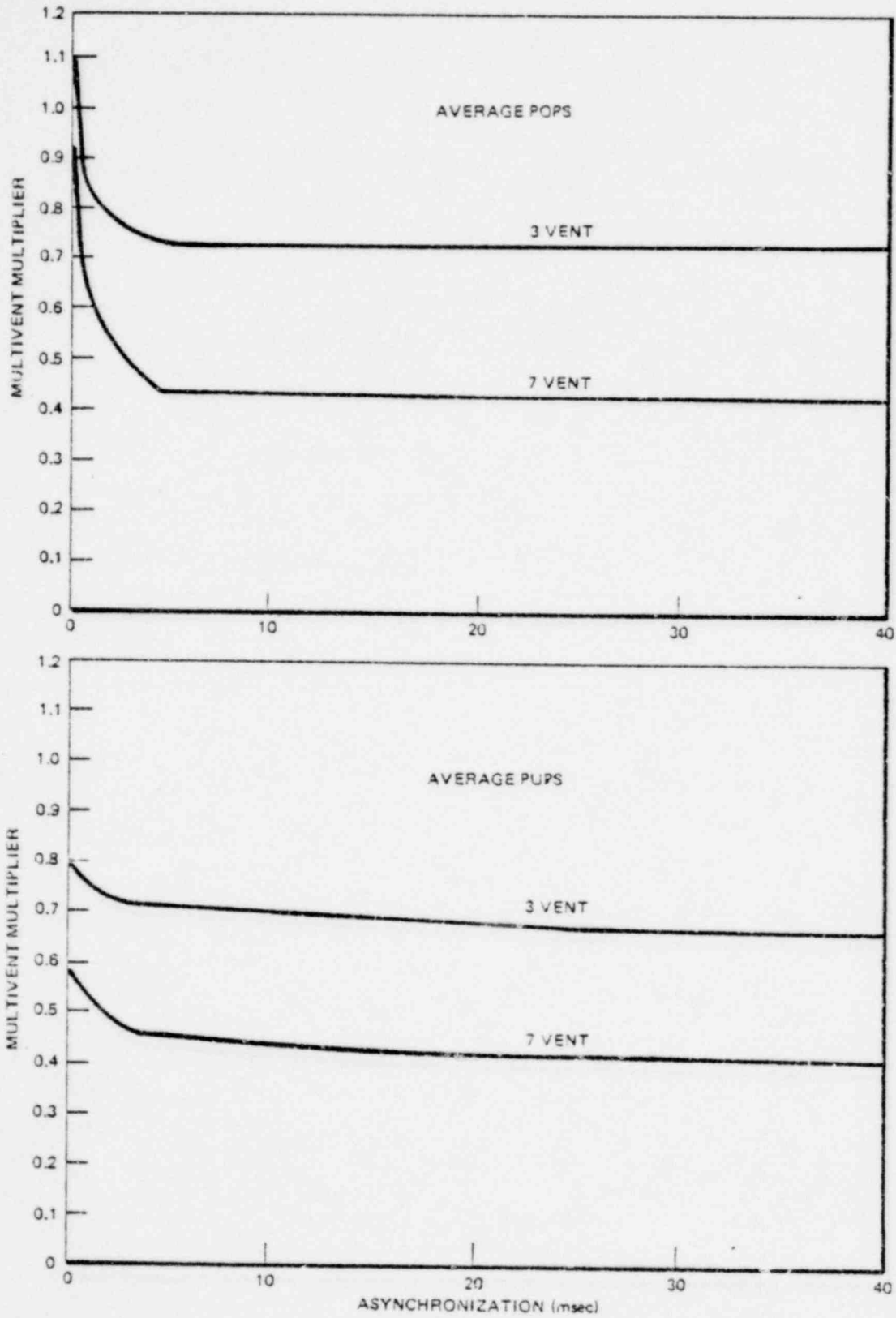


Figure 4-10. Test Series 3420, Sensitivity to Asynchronization

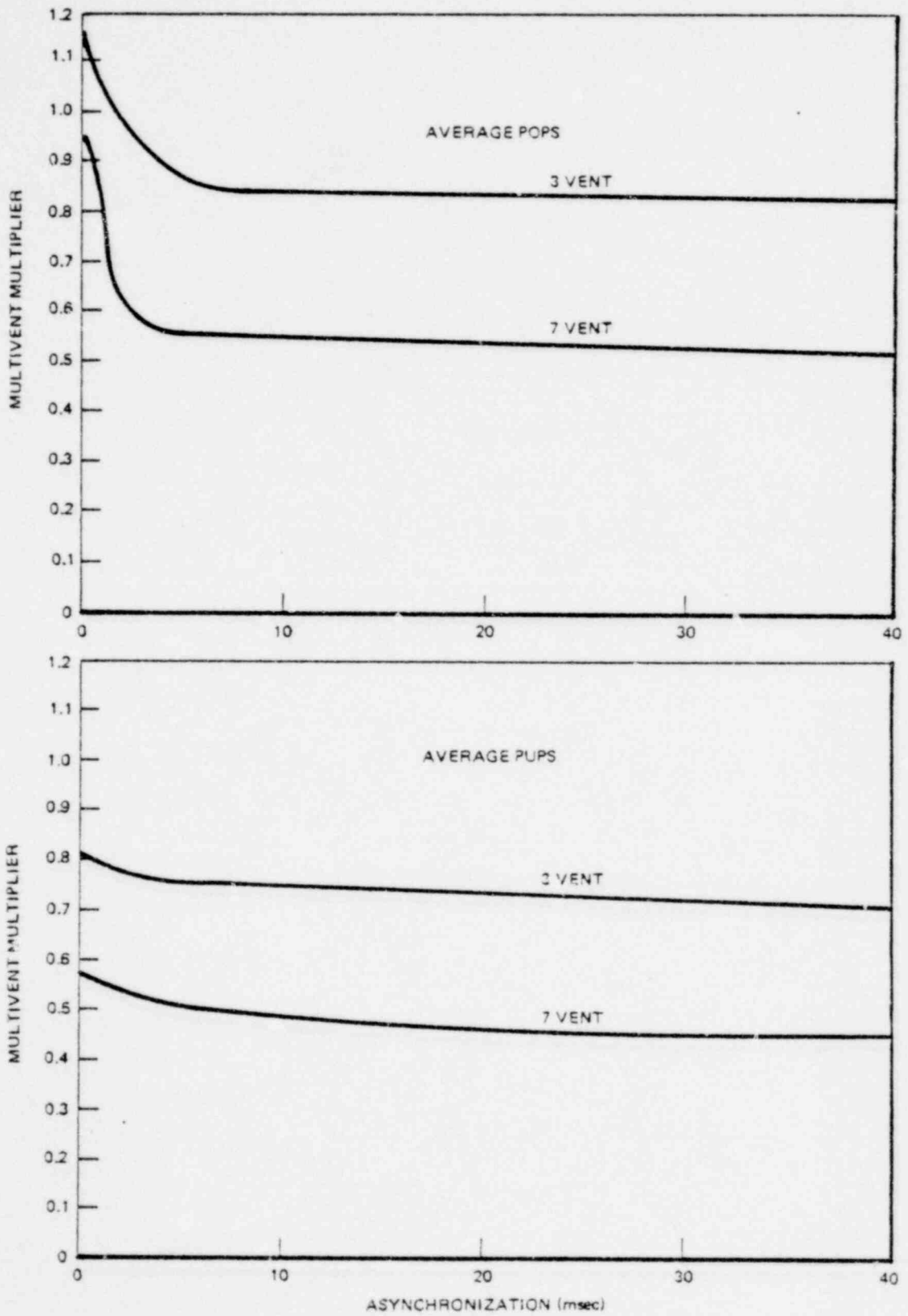


Figure 4-11. Test Series 3620, Sensitivity to Asynchronization

APPENDIX A  
DERIVATION OF PRESSURE FACTORS

In the calculation of source to wall pressure factors for the cylindrical test vessels a method of images type approach is used. An array of about 120 imaginary sources is created around the vessel. To take into account the free surface, this array is reflected through the plane of the free surface. A set of linear equations is developed describing the fluid velocity at certain points (nodes) on the vessel walls, as a function of the imaginary source strengths. The equations are then solved for the source strength which gives zero outward flow at the nodes. The imaging system is illustrated in Figure 3-1.

A.1 DERIVATION OF PRESSURE FACTOR EQUATIONS

In this derivation, the following notation is used:

$$q_{Rm} = \text{strength of } m\text{th real source } ft^3/sec^2$$

$$q_{In} = \text{strength of } n\text{th imaginary source } ft^3/sec^2$$

$$\bar{n}_j = \text{unit normal vector at } j\text{th node}$$

$$\bar{V}_j = \text{velocity vector at } j\text{th node}$$

$$\bar{V}_{Ijn} = \text{velocity vector at } j\text{th node due to the } n\text{th imaginary source}$$

$$\bar{V}_{Rjm} = \text{velocity vector at } j\text{th node due to the } m\text{th real source}$$

$$\bar{r}_{Rjm} = \text{distance vector from } m\text{th real source to } j\text{th node}$$

$$\bar{r}'_{Rjm} = \text{distance vector from } m\text{th real source reflection to } j\text{th node}$$

$$\bar{r}_{Ijn} = \text{distance vector from } n\text{th imaginary source to } j\text{th node}$$

$\vec{r}_{Ijn}$  = distance vector from nth imaginary source reflection to jth node.

nv = number of real source (vents)

nn = number of nodes and imaginary sources

The boundary condition of zero normal flow is specified at each node as,

$$\vec{v}_j \cdot \vec{n}_j = 0 \quad j = 1, nn \quad (A-1)$$

The velocity is broken into two components, one due to all real sources and another due to all imaginary sources

$$\vec{v}_j = \sum_{n=1}^{nn} \vec{v}_{Ijn} + \sum_{m=1}^{nv} \vec{v}_{Rjm} \quad (A-2)$$

Combining (A-1) and (A-2),

$$\sum_{n=1}^{nn} \vec{n}_j \cdot \vec{v}_{Ijn} + \sum_{m=1}^{nv} \vec{n}_j \cdot \vec{v}_{Rjm} = 0 \quad j = 1, nn \quad (A-3)$$

Taking the time derivative of (A-3)

$$\sum_{n=1}^{nn} \vec{n}_j \cdot \dot{\vec{v}}_{Ijn} + \sum_{m=1}^{nv} \vec{n}_j \cdot \dot{\vec{v}}_{Rjm} = 0 \quad (A-4)$$

The acceleration distribution due to a source in an infinite pool is given by

$$\vec{v} = \frac{\dot{q}\vec{r}}{4\pi|\vec{r}|^3}$$

The acceleration due to any single real or imaginary source, and its reflection (image sink above the free surface) is then,

$$\bar{v}_{Ijn} = \dot{q}_{In} \left[ \frac{\bar{r}_{Ijn}}{|\bar{r}_{Ijn}|^3} - \frac{\bar{r}'_{Ijn}}{|\bar{r}'_{Ijn}|^3} \right] \quad (A-5)$$

$$\bar{v}_{Rjm} = \dot{q}_{Rm} \left[ \frac{\bar{r}_{Rjm}}{|\bar{r}_{Rjm}|^3} - \frac{\bar{r}'_{Rjm}}{|\bar{r}'_{Rjm}|^3} \right] \quad (A-6)$$

Combining A-5 and A-6 with A-4

$$\sum_{n=1}^{nn} \dot{q}_{In} \left[ \frac{\bar{r}_{Ijn} \cdot \bar{n}_j}{|\bar{r}_{Ijn}|^3} - \frac{\bar{r}'_{Ijn} \cdot \bar{n}_j}{|\bar{r}'_{Ijn}|^3} \right] + \sum_{m=1}^{nv} \dot{q}_{Rm} \left[ \frac{\bar{r}_{Rjm} \cdot \bar{n}_j}{|\bar{r}_{Rjm}|^3} - \frac{\bar{r}'_{Rjm} \cdot \bar{n}_j}{|\bar{r}'_{Rjm}|^3} \right] \quad j = 1, nn \quad (A-7)$$

The equations represented by A-7 are put into matrix notation

$$AQ_I + BQ_R = 0 \quad (A-8)$$

where

$$Q_I = \begin{bmatrix} \dot{q}_{I1} \\ \dot{q}_{I2} \\ \vdots \\ \dot{q}_{Inn} \end{bmatrix} \quad Q_R = \begin{bmatrix} \dot{q}_{R1} \\ \dot{q}_{R2} \\ \vdots \\ \dot{q}_{Rnv} \end{bmatrix}$$

$$A = \begin{bmatrix} a_{11} & a_{12} & \cdots & a_{1 \text{ nn}} \\ a_{21} & a_{22} & \cdots & a_{2 \text{ nn}} \\ \vdots & \vdots & & \vdots \\ a_{\text{nn}1} & a_{\text{nn}2} & \cdots & a_{\text{nn} \text{ nn}} \end{bmatrix},$$

$$a_{jn} = \frac{\vec{r}_{Ijn} \cdot \vec{n}_i}{|\vec{r}_{Ijn}|^3} - \frac{\vec{r}'_{Ijn} \cdot \vec{n}_i}{|\vec{r}'_{Ijn}|^3}$$

$$B = \begin{bmatrix} b_{11} & b_{12} & \cdots & b_{1 \text{ nv}} \\ b_{12} & b_{22} & \cdots & b_{2 \text{ nv}} \\ \vdots & \vdots & & \vdots \\ b_{\text{nn}1} & b_{\text{nn}2} & \cdots & b_{\text{nn} \text{ nv}} \end{bmatrix},$$

$$b_{jm} = \frac{\vec{r}_{Rjm} \cdot \vec{n}_j}{|\vec{r}_{Rjm}|^3} - \frac{\vec{r}_{Rjn} \cdot \vec{n}_j}{|\vec{r}_{Rjn}|^3}$$

Since we have assumed the fluid in the vessel is incompressible and inviscous, and since the fluid velocities are small, we can write the time dependent Bernoulli equation as

$$\Delta P = \rho \frac{d\phi}{dt}$$

The velocity potential due to a source in a infinite pool is

$$\phi = \frac{q}{4\pi r}$$

1185 183

Then the pressure distribution due to a source in an infinite pool is

$$\Delta P = \frac{\rho}{4\pi} \frac{\dot{q}}{r}$$

The pressure due to all real and imaginary sources and their reflections at the kth node is

$$\Delta P_k = \frac{\rho}{4\pi} \left\{ \sum_{n=1}^{nn} \dot{q}_{In} \left[ \frac{1}{|\vec{r}_{Ikn}|} - \frac{1}{|\vec{r}'_{Ikn}|} \right] + \sum_{n=1}^{nv} \dot{q}_{Rn} \left[ \frac{1}{|\vec{r}_{Rkn}|} - \frac{1}{|\vec{r}'_{Rkn}|} \right] \right\}$$

In matrix notation this is

$$\Delta P_k = \frac{\rho}{4\pi} (R_{Ik} Q_I + R_{Rk} Q_R) \tag{A-9}$$

where

$$R_{Ik} = \begin{bmatrix} \frac{1}{|\vec{r}_{Ik1}|} - \frac{1}{|\vec{r}'_{Ik1}|}, & \frac{1}{|\vec{r}_{Ik2}|} - \frac{1}{|\vec{r}'_{Ik2}|}, & \dots, \\ \frac{1}{|\vec{r}_{Ik\ nn}|} - \frac{1}{|\vec{r}'_{Ik\ nn}|} \end{bmatrix}$$

$$R_{Rk} = \left[ \frac{1}{|\vec{r}_{Rk1}|} - \frac{1}{|\vec{r}'_{Rk1}|}, \frac{1}{|\vec{r}_{Rk2}|} - \frac{1}{|\vec{r}'_{Rk2}|}, \dots, \frac{1}{|\vec{r}_{Rk\text{ nv}}|} - \frac{1}{|\vec{r}'_{Rk\text{ nv}}|} \right]$$

Combining A-8 and A-9

$$\Delta P_k = \frac{\rho}{4\pi} \left[ R_R - R_I A^{-1} B \right] Q_R \tag{A-10}$$

This, then, gives the pressure factor matrix

$$F = \left[ f_1, f_2, f_3 \dots f_{\text{nv}} \right] = \frac{\rho}{4\pi} \left[ R_R - R_I A^{-1} B \right]$$

This completes the derivation of equation 5 in Subsection 2.1.1,

$$\Delta P_k = f_1 \dot{q}_{R1} + f_2 \dot{q}_{R2} + \dots + f_{\text{nv}} \dot{q}_{R\text{nv}} = F Q_R$$

## APPENDIX B

## SENSITIVITY OF IMAGE METHOD TO NODE NUMBER AND SOURCE POSITION

The pressure factors obtained by the imaging method will depend on the number of nodes used to define the vessel walls and the distance the imaginary sources are placed from the vessel. This, of course, is undesirable since the model results should be independent of internal details of the model. This dependence can be avoided by properly choosing these parameters.

Figure B-1 shows how the pressure factor for the single vent 1/10 scale test vessel depends on node number and distance to imaginary sources,  $D_s$ . With the imaginary sources placed 1/2 the vessel diameter from the vessel, the pressure factor is a strong function of node number below 120 nodes but is independent of node number above 120 nodes. With the sources placed one vessel diameter away this curve levels off much sooner, at 60 nodes. With  $D_s$  equal to two vessel diameters, the solution is unstable and cannot even be obtained with more than 64 nodes. This is because the matrix A becomes too ill-conditioned to invert.

Using 121 nodes and the distance from the imaginary sources to the vessel wall equal to 1 diameter, the pressure factor is not a function of these modeling parameters. This number of nodes was used for the MHM verification runs.

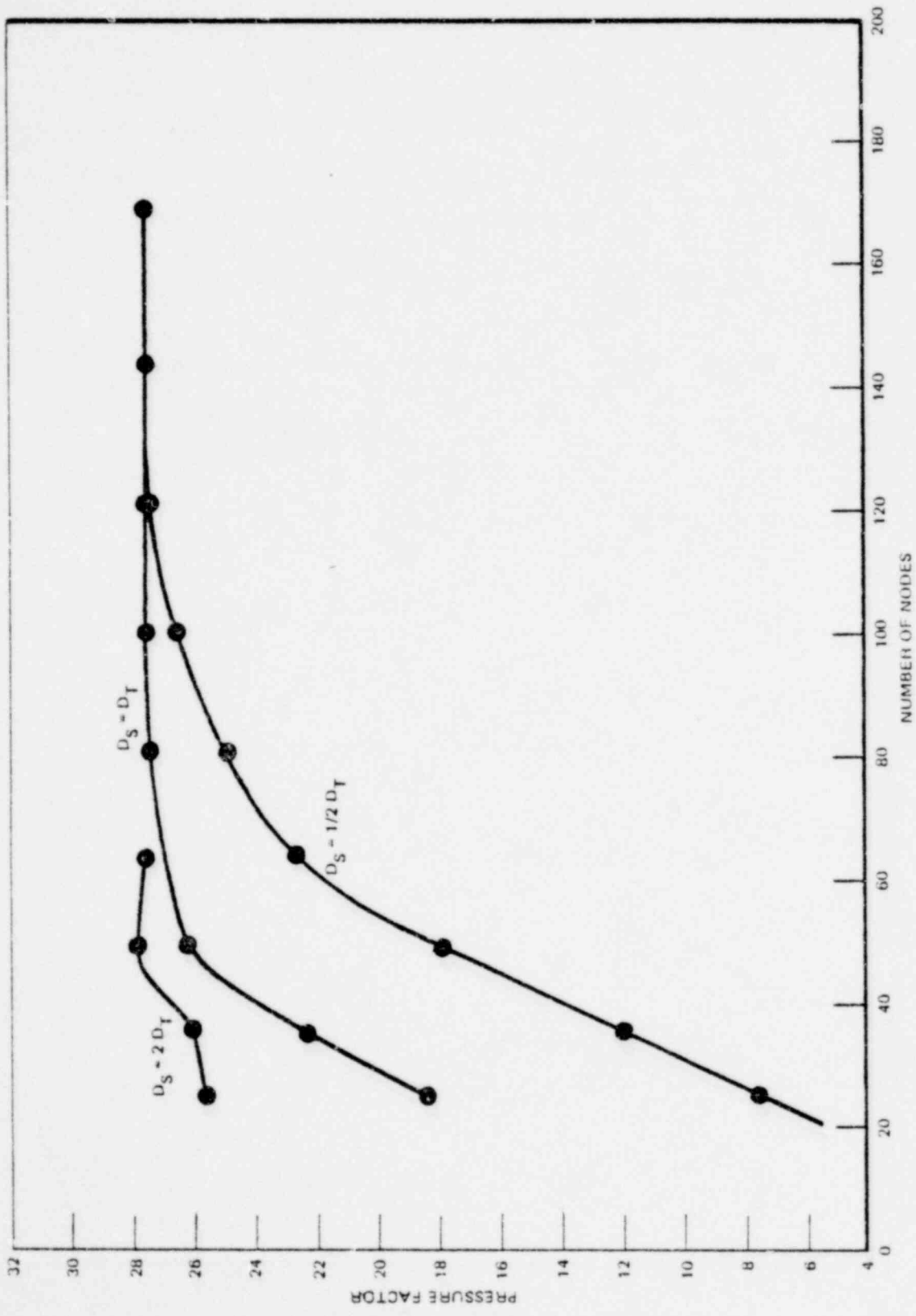


Figure B-1. Single Vent Pressure Factor Versus Node Number and Source Distance



TECHNICAL INFORMATION EXCHANGE

TITLE PAGE

AUTHOR	SUBJECT	TIE NUMBER 79NED105
A. P. Reese		DATE August 1979
TITLE A Comparison of the Mark II Multivent Hydrodynamic Model with Preliminary Results from the Scaled Multivent Test Program		GE CLASS I
		GOVERNMENT CLASS
REPRODUCIBLE COPY FILED AT TECHNICAL SUPPORT SERVICES, R&UO, SAN JOSE, CALIFORNIA 95125 (Mail Code 211)		NUMBER OF PAGES 44
SUMMARY		
In order to determine the wall pressure on a Mark II containment system during the chugging phase of a postulated LOCA, a model was developed which employs single vent chugging data and a Monte-Carlo technique to simulate multivent effects.		

By cutting out this rectangle and folding in half, the above information can be fitted into a standard card file.

DOCUMENT NUMBER NEDO-25116

INFORMATION PREPARED FOR Nuclear Energy Projects Division

SECTION Safety & Licensing

BUILDING AND ROOM NUMBER PYD 422 MAIL CODE 905

**POOR ORIGINAL**

**GENERAL  ELECTRIC**

1185 189